ISSN 1070-3284, Russian Journal of Coordination Chemistry, 2024, Vol. 50, No. 7, pp. 500–511. © Pleiades Publishing, Ltd., 2024.

Coordination Compounds of 3*d* Metals with 2,4-Dimethylpyrazolo[1,5-a]benzimidazole: Magnetic and Biological Properties

O. G. Shakirova[a, b], T. A. Kuz'menko[c], N. V. Kurat'eva[a], L. S. Klyushova[d], A. N. Lavrov[a], and L. G. Lavrenova[a, *, **]

[a] *Nikolaev Institute of Inorganic Chemistry, Siberian Branch, Russian Academy of Sciences, Novosibirsk, Russia*

[b] *Komsomolsk-on-Amur State University, Komsomolsk-on-Amur, Russia*

[c] *Institute of Physical and Organic Chemistry, Southern Federal University, Rostov-on-Don, Russia*

[d] *Institute of Molecular Biology and Biophysics, Federal Research Center for Fundamental and Translational Medicine, Novosibirsk, Russia*

**e-mail: ludm@niic.nsc.ru*

***e-mail: Shakirova_Olga@mail.ru*

Received December 26, 2023; revised April 10, 2024; accepted April 22, 2024

Abstract—New coordination compounds of copper(I), copper(II), cobalt(II), and nickel(II) with 2,4-dimethylpyrazolo[1,5-a]benzimidazole (L) were synthesized and studied. The complexes [CuLCl] (**I**), [CuLBr] (**II**), $[CuL_2Cl_2]$ (**III**), $[CuL_2(NO_3)_2]\cdot H_2O$ (**IV**), $[CoL_2Cl_2]\cdot 0.5H_2O$ (**V**), $[CoL_2(NO_3)_2]\cdot 0.5H_2O$ (**VI**), and $[NiL_2(NO_3)_2]\cdot 0.5H_2O$ (**VII**) were studied by IR spectroscopy and powder and single crystal X-ray diffraction (CCDC nos. 2321779 ($[CuL_2Cl_2]$), 2321780 ($[CoL_2(NO_3)_2]$)). The results indicate that the coordination polyhedron in 2,4-dimethylpyrazolo[1,5-a]benzimidazole complexes is formed by the nitrogen atoms of the monodentate ligand and the coordinated anion. The cytotoxic and cytostatic properties of L and complexes **I**–**III** were studied in relation to the HepG2 hepatocellular carcinoma cells.

Keywords: synthesis, coordination compounds, 3*d* metals, 2,4-dimethylpyrazolo[1,5-a]benzimidazole, powder and single crystal X-ray diffraction, UV/Vis and IR spectroscopy, magnetic susceptibility, in vitro assay, HepG2

DOI: 10.1134/S1070328424600621

INTRODUCTION

Polynitrogen-containing heterocyclic compounds represent a promising class of ligands for the synthesis of transition metal complexes possessing biological activity [1–3]. Benzimidazole and its derivatives exhibit a wide range of pharmacological properties. The complex formation of biologically important organic compounds with metal ions may markedly increase their efficiency in comparison with the free organic ligand. Coordination compounds of transition metals with benzimidazoles exhibit antibacterial, antiparasitic, anti-inflammatory, antiviral, and antitumor effects [4–15]. Copper(II) chloride complexes with ligands of this class mimic the activity of superoxide dismutase (SOD), which is one of the major enzymes of the antioxidant system. Metalloenzymes, among which Cu,Zn-SOD has a relatively high activity, catalyze disproportionation of superoxide radical anions and reduce the probability of formation of even more active singlet oxygen [16, 17]. In addition, SOD plays an important role in the antiaging mechanisms [18, 19].

Previously, our research team prepared a series of complexes of copper(II) halides with 4*H*-1,2,4-triazolo[1,5-a]benzimidazole, 3-methyl-1,2,4-triazolo-[1,5-a]benzimidazole, 4-methyl-1,2,4-triazolo-[1,5-a]-benzimidazole, 2,4-dimethyl-1,2,4-triazolo-[1,5-a]-benzimidazole, 2-methyl-1,2,4-triazolo[1,5-a]benzimidazole, and 2-(3,5-dimethylpyrazol-1-yl)benzimidazole. The cytotoxic action of the complexes and ligands on the Hep-2 cell line was studied. It was found that formation of copper(II) complexes with these ligands significantly enhances their cytotoxicity [20–24]. The obtained $[CuLCl_2]$ complex with 2-(3,5-dimethylpyrazol-1-yl)benzimidazole is comparable with cisplatin in the cytotoxic action [24]. It seemed reasonable to continue research along this line.

The purpose of this study was to obtain new coordination compounds of copper(II), cobalt(II), and nickel(II) and to evaluate their biological and mag-

Table 1. Results of elemental analysis of complexes **I**–**VII**

Compound	Molecular formula	Found/calcd., %		
		C	H	N
[CuLCl] (**I**)	$C_{11}H_{11}ClCuN_3$	46.1/46.5	3.8/3.9	14.5/14.8
[CuLBr] (**II**)	$C_{11}H_{11}BrCuN_3$	40.7/40.2	3.4/3.4	12.4/12.8
$[CuL_2Cl_2]$ (**III**)	$C_{22}H_{22}Cl_2CuN_6$	53.5/52.3	4.5/4.4	16.4/16.6
$[CuL_2(NO_3)_2]\cdot H_2O$ (**IV**)	$C_{22}H_{24}CuN_8O_7$	46.4/45.9	4.0/4.2	19.3/19.5
$[CoL_2Cl_2]\cdot 0.5H_2O$ (**V**)	$C_{22}H_{23}Cl_2CoN_6O_{0.5}$	53.7/51.9	4.4/4.6	16.4/16.5
$[CoL_2(NO_3)_2]\cdot 0.5H_2O$ (**VI**)	$C_{22}H_{22}CoN_8O_{6.5}$	47.6/47.0	4.0/4.1	19.9/19.9
$[NiL_2(NO_3)_2]\cdot 0.5H_2O$ (**VII**)	$C_{22}H_{22}NiN_8O_{6.5}$	48.6/47.0	4.1/4.1	19.7/19.9

netic activities. 2,4-Dimethylpyrazolo[1,5-a]benzimidazole (L) was used as the ligand for the synthesis (Scheme 1).

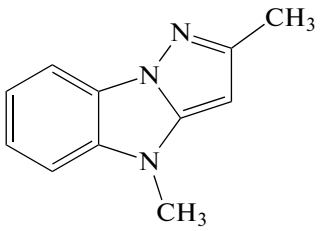

Scheme 1.

EXPERIMENTAL

Commercially available chemicals and solvents were used as received. 2,4-Dimethylpyrazolo[1,5-a]benzimidazole (L,$C_{11}H_{11}N_3$) was prepared by a reported procedure [25].

Synthesis of [CuLCl] (I). Portions of the ligand L (0.19 g, 1.0 mmol) and $CuCl_2\cdot 2H_2O$ (0.17 g, 1.0 mmol) were dissolved separately in ethanol (5 mL). The salt solution was added to the solution of the ligand, this gave a violet-colored solution, from which a white solid rapidly precipitated. The precipitate was collected on a filter, washed with ethanol several times, and dried in air. All of the obtained compounds were dried in a similar way. The yield was 0.08 g (28%).

Synthesis of [CuLBr] (II). Portions of $CuBr_2$ (0.22 g, 1.0 mmol) and ligand L (0.37 g, 2.0 mmol) were dissolved separately in ethanol or acetone (5 mL). Then a solution of $CuBr_2$ in ethanol or acetone (5 mL) was added to the solution of the ligand. At any metal to ligand ratio and in both solvents, the brown solution was immediately decolorized, and a white solid precipitated. The precipitate was collected on a filter and washed several times with the appropriate solvent. The yield was 0.30–0.32 g (91–97%) in ethanol and 0.18–0.20 g (55–61%) in acetone.

Synthesis of $[CuL_2Cl_2]$ (III). A portion of ligand L (0.09 g, 0.5 mmol) was dissolved in acetone (5 mL). A solution of $CuCl_2\cdot 2H_2O$ (0.19 g, 1.0 mmol) in acetone (5 mL) was added to the solution of L. This gave a dark red solution. A gray-black precipitate was formed when the solution volume was halved during the slow evaporation of acetone. The precipitate was collected on a filter, washed with acetone several times (the color of the precipitate did not change), and dried in air. The yield was 0.17 g (67%). In the mother liquor left overnight, dark red crystals of $[CuL_2Cl_2]$ (**III**) suitable for X-ray diffraction precipitated.

Synthesis of $[CuL_2(NO_3)_2]\cdot H_2O$ (IV), $[CoL_2Cl_2]\cdot 0.5H_2O$ (V), $[CoL_2(NO_3)_2]\cdot 0.5H_2O$ (VI), and $[NiL_2(NO_3)_2]\cdot 0.5H_2O$ (VII). A portion of ligand L (0.37 g, 2.0 mmol) was dissolved in acetone (5 mL). A solution of $CoCl_2\cdot 6H_2O$ (0.24 g, 1.0 mmol), or $Co(NO_3)_2\cdot 6H_2O$ (0.29 g), or $Ni(NO_3)_2\cdot 6H_2O$ (0.29 g), or $Cu(NO_3)_2\cdot 3H_2O$ (0.24 g) in acetone (5 mL) was added to the resulting solution of L. This gave a brown (**IV**), blue (**V**), lilac (**VI**), or light green (**VII**) solution, in which precipitates of the same color as the solution were rapidly formed. The precipitates were collected on a filter and washed with ethanol several times. The yields were 0.30 g (52%) for **IV**; 0.37 g (72%) for **V**; 0.33 g (59%) for **VI**; and 0.20 g (36%) for **VII**.

Elemental analysis for C, H, and N was performed at the analytical laboratory of the Nikolaev Institute of Inorganic Chemistry, Siberian Branch, Russian Academy of Sciences, on a EURO EA 3000 instrument (EuroVector, Italy). The results of the analysis are summarized in Table 1.

X-ray diffraction study of $[CuL_2Cl_2]$ and $[CoL_2(NO_3)_2]$ was carried out according to the standard procedure on a Bruker-Nonius X8Apex four-circle automated diffractometer equipped with a CCD array detector, at 150 K using molybdenum radiation (λ = 0.71073 Å) and a graphite monochromator. The reflection intensities were measured by φ- and ω-scanning of narrow (0.5°) frames. The absorption corrections were applied empirically by the SADABS program [26]. The structures were solved by direct methods and refined by full-matrix least-squares calculations in the anisotropic approximation for non-hydrogen atoms using the SHELXTL program pack-

Table 2. Crystallographic data and X-ray experiment and structure refinement details for the complexes $[CuL_2Cl_2]$ and $[CoL_2(NO_3)_2]$

Parameter	Value	
	$[CuL_2Cl_2]$	$[CoL_2(NO_3)_2]$
Molecular formula	$C_{22}H_{22}Cl_2CuN_6$	$C_{22}H_{22}CoN_8O_6$
M	504.89	553.40
System	Monoclinic	Triclinic
Space group	$C2/c$	$P\bar{1}$
a, Å	14.1769(8)	7.8732(3)
b, Å	7.9398(4)	10.6968(4)
c, Å	20.1106(14)	15.1802(6)
α, deg	90	87.907(2)
β, deg	108.566(2)	75.202(2)
γ, deg	90	68.805(1)
Volume, Å^3	2145.9(2)	1150.22(8)
Z	4	2
ρ(calcd.), g/cm^3	1.563	1.598
μ(MoK_α), mm^{-1}	1.290	0.805
F(000)	1036	570
Crystal size, mm	0.42 × 0.35 × 0.08	0.30 × 0.21 × 0.09
Data collection range of θ	2.137–26.363	1.390–26.420
Range of indices h,k,l	$-17 \le h \le 17$, $-6 \le k \le 9$, $-25 \le l \le 25$	$-9 \le h \le 9$, $-13 \le k \le 13$, $-18 \le l \le 18$
Number of measured reflections	7630	9166
Number of unique reflections (R_{int})	2183 (0.0316)	4652 (0.0345)
Completeness of data collection at θ = 25.25°, %	99.6	98.9
Number of reflections/restraints/parameters	2183/0/143	4652/0/339
S-factor on F^2	1.036	1.054
R_1, wR_2 ($I > 2\sigma(I)$)	0.0469, 0.1172	0.0437, 0.0851
R_1, wR_2 (all data)	0.0545, 0.1218	0.0562, 0.0889
Residual electron density (max/min), e/Å^3	1.475/–0.510	0.633/–0.421

age [27]. The hydrogen atoms were refined in the rigid-body approximation. The crystallographic data and X-ray experiment details are given in Table 2, and selected interatomic distances and bond angles are in Table 3.

The crystallographic parameters of the $[CuL_2Cl_2]$ and $[CoL_2(NO_3)_2]$ structures were deposited with the Cambridge Crystallographic Data Centre (nos. CCDC 2321779 and 2321780, respectively; https://www.ccdc.cam.ac.uk/data_reguest/cif).

The powder X-ray diffraction study of the polycrystalline compounds was performed on a Shimadzu XRD 7000 diffractometer (CuK_α radiation, Ni filter, scintillation detector) at room temperature.

IR absorption spectra were measured on Scimitar-FTS 2000 and Vertex 80 spectrometers in the 4000–100 cm^{-1} range. The samples were prepared as pastes in mineral or fluorinated oil and in polyethylene at room temperature.

Diffuse reflectance spectra were recorded on a UV-3101 PC scanning spectrophotometer (Shimadzu) at room temperature.

The magnetic properties were measured on a MPMS-*XL* SQUID magnetometer (Quantum Design) in the temperature range of 1.77–300 K and magnetic fields H of 0–10 kOe. The paramagnetic component of the molar magnetic susceptibility ($\chi_p(T)$) was determined by subtracting the diamagnetic contribution χ_d and possible ferromagnetic contribution of trace impurities χ_{FM} from the measured full magnetic susceptibility $\chi = M/H$ (M = magnetization). The temperature-independent contribution χ_d

Table 3. Selected interatomic distances (*d*, Å) in the coordination units of $[CuL_2Cl_2]$ and $[CoL_2(NO_3)_2]$*

$[CuL_2Cl_2]$		$[CoL_2(NO_3)_2]$	
d, Å		*d*, Å	
Cu(1)–N(1)	1.975(3)	Co(1)–N(11)	2.051(2)
Cu(1)–N(1)$^{\#1}$	1.975(3)	Co(1)–O(11)	2.0525(19)
Cu(1)–Cl(1)$^{\#1}$	2.2676(8)	Co(1)–N(21)	2.060(2)
Cu(1)–Cl(1)	2.2676(8)	Co(1)–O(22)	2.089(2)
		Co(1)–O(21)	2.256(2)
		Co(1)–O(12)	2.308(2)

* Symmetry code: $^{\#1}$ $-x + 1, y, -z + 1/2$.

was calculated by the Pascal additive scheme. The ferromagnetic contribution χ_{FM} was determined by measuring the field dependences $M(H)$ and the temperature dependences $M(T)$ at different magnetic field strengths followed by separation of the total sample magnetization into ferromagnetic and paramagnetic components. For the sample, the ferromagnetic contribution to the magnetization at $H = 10$ kOe did not exceed 0.01 and 2% at $T = 1.77$ and 300 K, respectively.

The cytotoxic and cytostatic activity of the synthesized compounds was evaluated using the HepG2 human hepatocellular carcinoma cell line by double staining with Hoechst 33342/propidium iodide (PI) fluorescent dyes [28]. The cells were seeded into 96-well plates (5×10^3 cells per well) in the IMDM nutrition medium (Sigma-Aldrich, United States) containing 10% fetal bovine serum (HyClone, United States) and were cultured for 24 h under standard conditions (moist atmosphere, 5% CO_2, 37°C). The complexes were dissolved in ethanol with the addition of DMSO, and working solutions were prepared by serial dilutions with the IMDM medium; the final concentration of EtOH was <1%. The cells were treated with the test compounds (1–50 μmol L^{-1}), incubated for 48 h, and stained with Hoechst 33342 (Sigma-Aldrich, Switzerland) and propidium iodide (Invitrogen, United States) for 30 min at 37°C. The measurements were carried out on an IN Cell Analyzer 2200 instrument (GE Healthcare, UK) in the automatic mode using 4 fields per well. The obtained images were analyzed with the In Cell Investigator software (GE Healthcare, UK) to determine live, dead, and apoptotic cells in the whole population. The results were presented as the percentages of cells from three wells ± root-mean-square deviation.

RESULTS AND DISCUSSION

The Cu(II), Co(II), and Ni(II) coordination compounds **I**–**VII** were prepared by reactions between ethanol or acetone solutions of salts and the ligand L. In ethanol, the complex formation was accompanied by reduction of copper(II) to copper(I), which resulted in isolation of the complexes [CuLCl] (**I**) and [CuLBr] (**II**).

All of the obtained complexes were stable in air and at room temperature over a long period of time and non-hygroscopic. They were readily soluble in acetone and dichloromethane, much less soluble in ethanol, and virtually insoluble in water.

For the Cu : L ratio of 1 : 2, a dark gray precipitate was isolated from the solution. According to the results of magnetic susceptibility measurements, the product contained both copper(I) and copper(II). During the reduction of copper(II), a part of the ligand was oxidized and was simultaneously condensed with the solvent (Scheme 2) to form 1-(2,4-dimethylpyrazolo[1,5-a]benzimidazol-3-yl)ethanone (L*, $C_{13}H_{13}N_3O$).

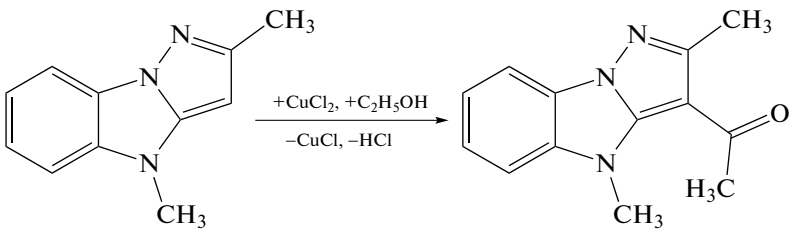

Scheme 2. Conversion of 2,4-dimethylpyrazolo[1,5-a]benzimidazole to 1-(2,4-dimethylpyrazolo[1,5-a]benzimidazol-3-yl)ethanone.

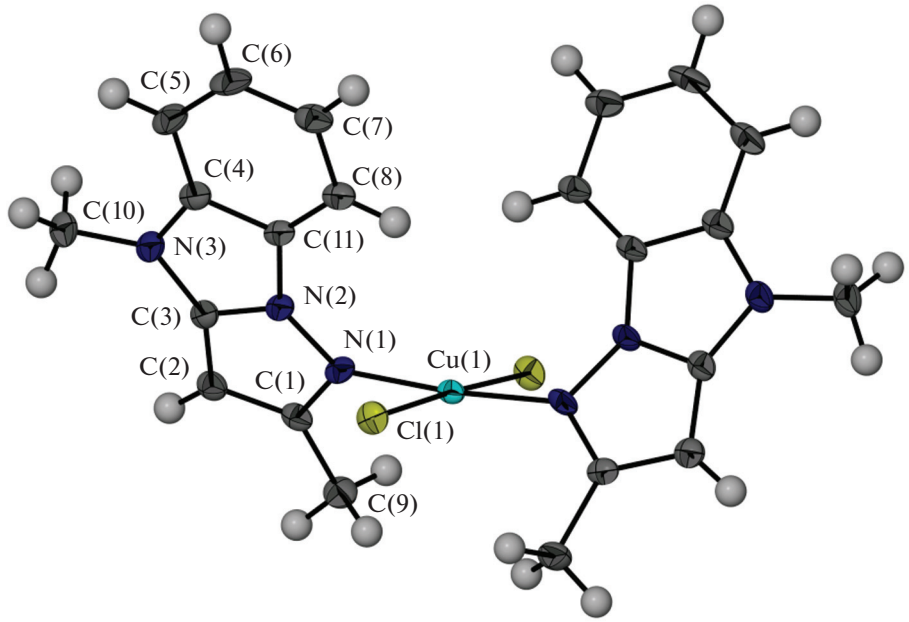

Fig. 1. Molecular structure of $[CuL_2Cl_2]$.

After the dark gray precipitate was filtered off, dark red crystals of $[CuL_2Cl_2]$ (**III**), suitable for X-ray diffraction, were formed in the mother liquor within 24 h (see Table 1, Fig. 1).

According to X-ray diffraction data, complex **III** crystallizes in the monoclinic system (Table 2). The independent part of the unit cell contains a half of molecular complex **III**, and the position of Cu atom coincides with a twofold axis along the *b* parameter (Fig. 2). The structure is of island molecular type. The neutral molecular complex $[CuL_2Cl_2]$ contains a Cu^{2+} cation, two coordinated Cl^- anions, and two L molecules coordinated to Cu^{2+} as monodentate ligands via a pyrazole nitrogen atom. The Cu^{2+} ion has a distorted square planar coordination polyhedron (Fig. 1), with the distortion being mainly caused by the different lengths of the Cu–Cl and Cu–N contacts (Table 3), while the ClCuN angles are close to 90°.

The packing of molecular complexes can be conceived as a distorted ABAB type hexagonal sphere packing along the *c* parameter (Fig. 3). The Cu...Cu distances within this pseudo-hexagonal layer vary in the range of 7.940–8.124(1) Å, while the CuCuCu angles for the most proximate centers of complex species vary in the 58.5°–60.75° range, indicating a minor packing distortion according to the external shape of the particles. Alignment of the planar parts of the organic ligands of neighboring molecular complexes is also observed, but no real stacking is present due to the significant displacement of the aromatic systems relative to one another.

The single crystals of the anhydrous complex, suitable for X-ray diffraction, were obtained by recrystallization of $[CoL_2(NO_3)_2]\cdot 0.5H_2O$ (**VI**) from acetone. According to X-ray diffraction data, the complex $[CoL_2(NO_3)_2]$ crystallizes in the triclinic system (Table 2). In the independent part of the cell, a complete complex molecule occurs in a general position of the space group (Fig. 4). Like complex **III**, this is also an island molecular structure (Fig. 5). The pseudo-octahedral CoN_2O_4 coordination unit is formed by two ligand L molecules monodentately bound to Co^{2+} via a pyrazole nitrogen atom and by two bidentate nitrate ions (Fig. 4).

The packing of molecular fragments can also be described as a highly distorted hexagonal packing along the *c* parameter, but in this case, it corresponds

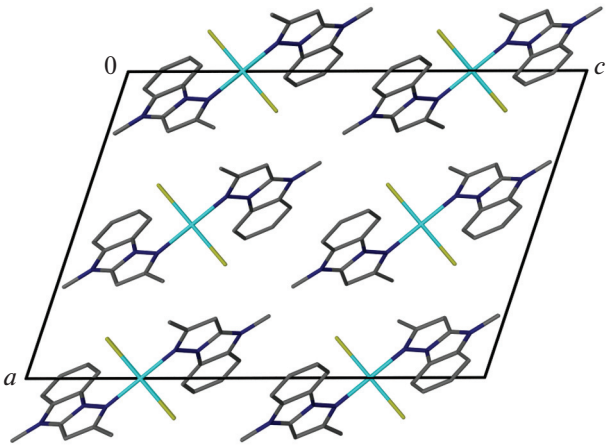

Fig. 2. Crystal structure of $[CuL_2Cl_2]$.

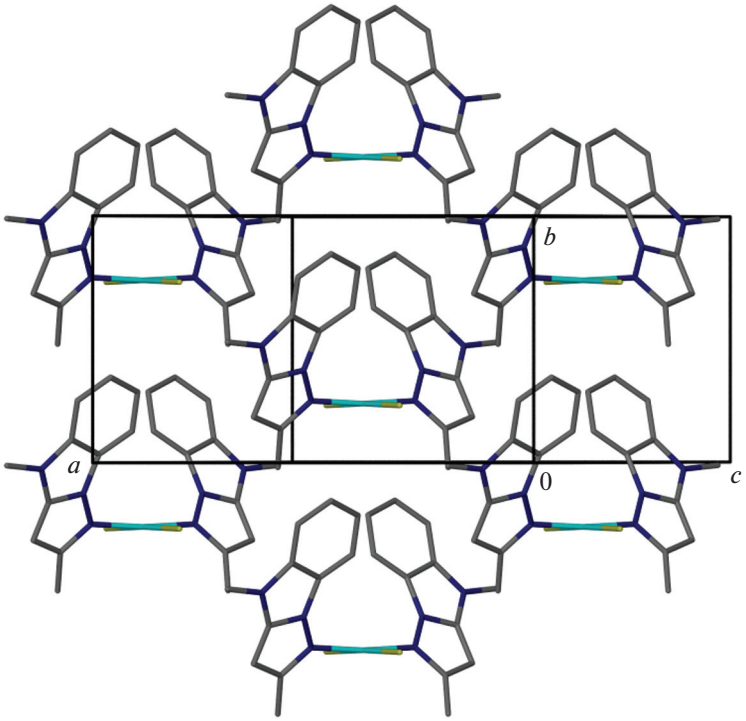

Fig. 3. Hexagonal motif of packing of the molecular complexes $[CuL_2Cl_2]$ shown in the *ab* plane (H are omitted for clarity).

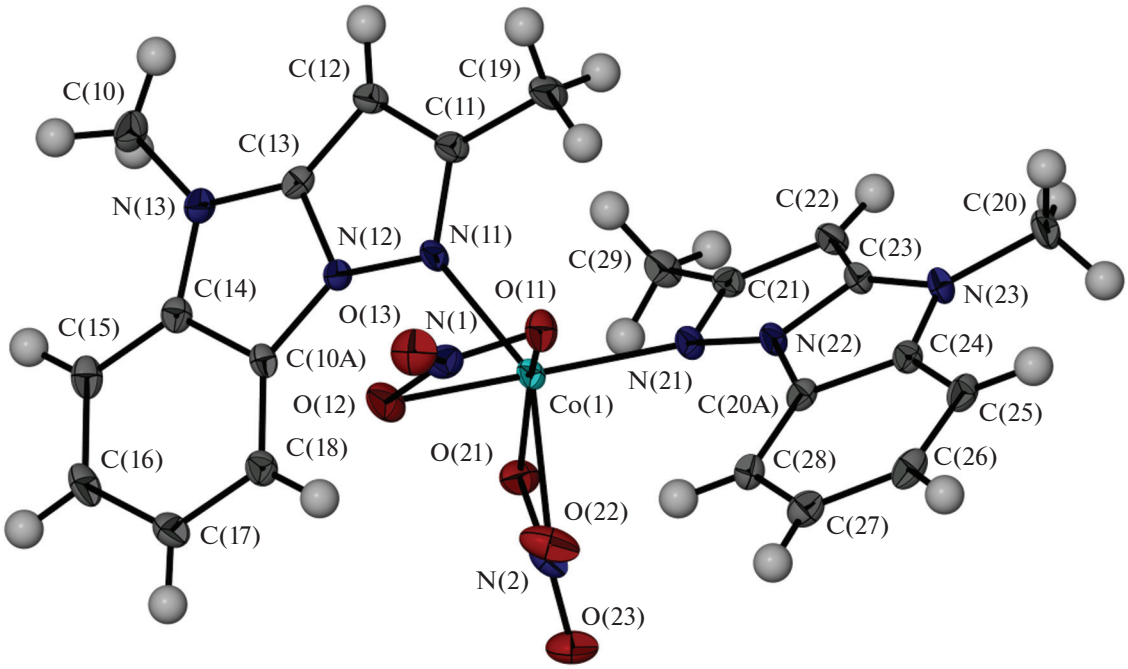

Fig. 4. Molecular structure of $[CoL_2(NO_3)_2]$.

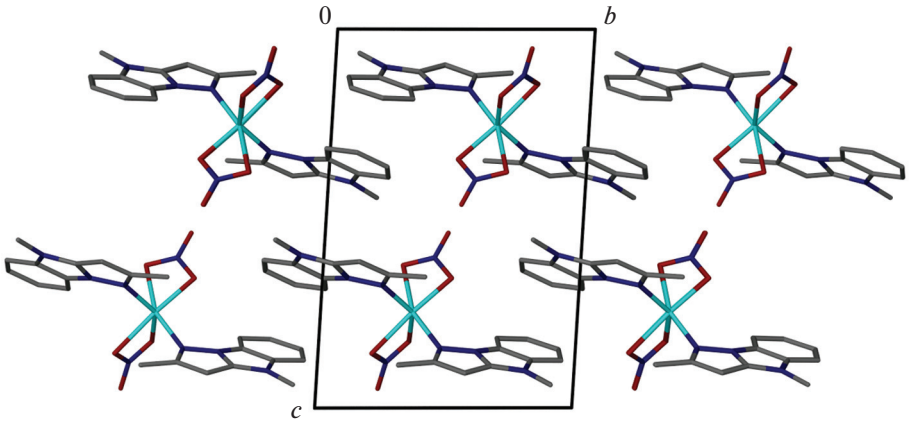

Fig. 5. Crystal structure of $[CoL_2(NO_3)_2]$.

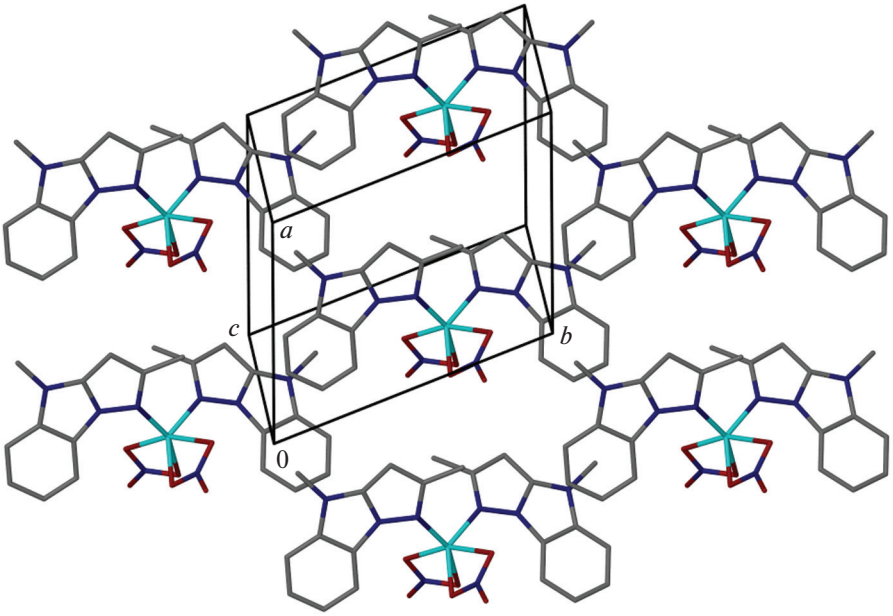

Fig. 6. Hexagonal motif of packing of the molecular complexes $[CoL_2(NO_3)_2]$ shown in the *ab* plane (H are omitted for clarity).

to the AAAA type (Fig. 6), with the distances between the centers of the molecular complexes being 7.873–10.748 Å. In this case, stacking is also hindered by the significant displacement of the aromatic moieties of neighboring molecular complexes and the presence of non-planar methyl substituents exactly on the side of possible stacking.

Analysis of powder X-ray diffraction data indicates that all complexes are crystalline (Figs. 7, 8). However, the complexes with equal numbers of ligands, [CuLA] (A = Cl^-, Br^-) and $[ML_2A_2]$ (M = Co, Ni, Cu; A = Cl^-, NO_3^-), are not isostructural.

The IR spectrum of L exhibits bands for the ν(C–H) stretching vibrations in the 3200–2800 cm^{-1} range and coordination-sensitive vibrations of the pyrazolo[1,5-a]benzimidazole core at 1690–1400 cm^{-1}. In the spectra of the copper chloride complexes, the pyrazole and imidazole stretching bands are shifted by ~30 cm^{-1} to higher frequency with respect to those in the L molecule, indicating that the pyrazole nitrogen atoms are coordinated to the metal [29] (Table 4). It is noteworthy that the vibrational bands of the nitrate ion (ν_5 in the 1620–1490 cm^{-1} range; ν_1 in the 1290–1160 cm^{-1} range; and ν_2 in the 1040–990 cm^{-1} range) are completely covered by the R and δ(C–H) bands of the heterocycles, which precludes determination of the coordination mode of this anion from the IR spectroscopy data.

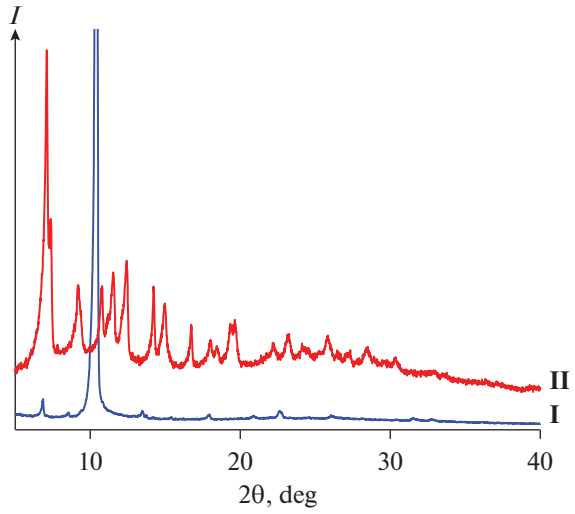

Fig. 7. X-ray diffraction patterns for the complexes [CuLHal].

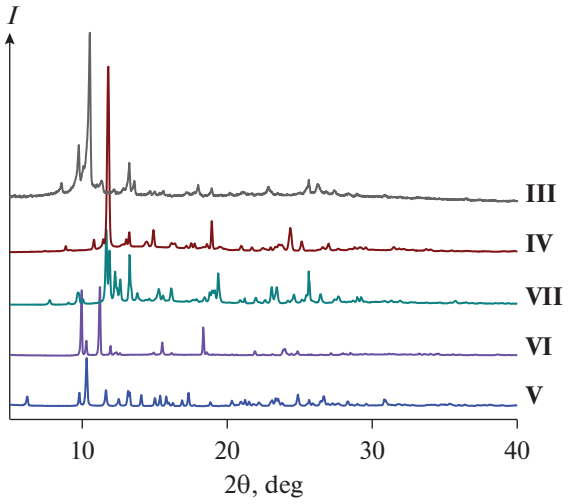

Fig. 8. X-ray diffraction patterns for the complexes $[ML_2A_2]$.

The low-frequency part (400–100 cm^{-1}) of the spectrum of L shows the δ(C–H) bending modes of the ligand (429, 363, 322, 288, 238, 194, 142, and 110 cm^{-1}), which shift only slightly in the spectra of complexes **I**–**III** (~3–5 cm^{-1}). In addition, the spectra of **I**–**III** exhibit low-intensity ν(Cu–N) bands at 400 cm^{-1} (for **I** and **III**) or at 394 cm^{-1} (for **II**); δ(Cu–N) bands at 247 cm^{-1} (**I** and **II**) or at 248 cm^{-1} (**III**); and stretching bands for the terminal Cu–Cl bonds at 280 (**I**) or 282 cm^{-1} (**III**) and Cu–Br bonds at 223 cm^{-1} (**II**).

In the diffuse reflectance spectra of complexes **V**–**VII** (Table 5), broad absorption bands are present in the range of 200–1000 nm; this position is characteristic of the spectra of cobalt(II) and nickel(II) complexes with nitrogen-containing ligands [30].

These results imply that complex **V** has a tetrahedral geometry, while Co(II) and Ni(II) nitrate complexes have a distorted octahedral geometry of the coordination polyhedron. The crystal field splitting parameters were calculated for these complexes. For complex **V**, the calculation was performed using Appendix V of the monograph [30] (Table V.1) and gave $B = 830$ cm^{-1} and $10Dq = 7473$ cm^{-1}. In the case of **VI**, the 10Dq value was calculated from the condition $\nu_1 = 8.8Dq$ and amounted to 12153 cm^{-1}; for **VII**, $10Dq = \nu_1 = 10846$ cm^{-1}. These Dq values indicate that the coordination units of **VI** and **VII** incorporate both nitrogen and oxygen atoms. This is confirmed by X-ray diffraction data for $[CoL_2(NO_3)_2]$.

The magnetochemical study of a sample of **III** revealed paramagnetic behavior over the whole temperature range of 1.77– 300 K (Fig. 9). In the range $T = 20$–300 K, the temperature dependence of the magnetic susceptibility measured in $H = 1$, 10 kOe fields was well described by the Curie–Weiss law $\chi_p(T) = N_A\mu_{eff}^2/3k_B(T-\theta)$ with the effective magnetic moment $\mu_{eff} \approx 1.76\ \mu_B$ and the Weiss constant $\theta \approx -0.4$ K. This μ_{eff} value is close to the theoretical spin-only value $\mu_{eff}(Cu^{2+}) \approx 1.73\ \mu_B$ for Cu^{2+} ions ($S = 1/2$), and the value of the Weiss constant corresponds to the weak antiferromagnetic (AFM) exchange interaction J between the Cu^{2+} ions. In the mean-field model for isotropic exchange interaction, θ is described by the expression $\vartheta = zJ\dfrac{2S(S+1)}{3k_B}$, where z is the number of nearest neighbors in the magnetic sublattice, k_B is the Boltzmann's constant. Thus, in this approximation, $zJ/k_B \approx 0.8$ K.

Detailed analysis of the low-temperature $\chi_p(T)$ data shows that at $T < 20$ K, the magnetic susceptibility deviates from the Curie–Weiss law toward larger values, which usually indicates a one-dimensional chain nature of exchange interactions [31]. Indeed, over a broad temperature range of 1.77–300 K, the curve $\chi_p(T)$ is in better agreement not with the Curie–Weiss law, but instead with the Bonner–Fisher dependence [32] for antiferromagnetic ($S = 1/2$) chains described by the Hamiltonian $H = J_{ch}\sum_i \vec{S}_i \cdot \vec{S}_{i+1}$ with the parameter $J_{ch}/k_B \approx 0.5$ K, characterizing the exchange interaction between the Cu^{2+} ions within the chain. This type of magnetic behavior may indicate a specific packing of molecules in the crystal lattice in which the exchange interaction between the Cu^{2+} ions is mainly implemented along only one crystallographic direction.

Additional information on the magnetic state of copper ions in sample **III** can be derived from the field dependence of the magnetization (Fig. 10). The

Table 4. Wave numbers (frequencies, cm^{-1}) of the absorption maxima in the IR spectra of L and complexes **I**–**VII**

Assignment	L	**I**	**II**	**III**	**IV**	**V**	**VI**	**VII**
ν (O–H)					3415	3445	3437	3437
ν (C_{ring}–H)	3125, 3019	3125, 3017	3125, 3061	3076, 3017	3142, 3057	3175	3180	3175
ν_{as} (CH_3)	2924	2905	2906	2914	2940	2926	2923	2922
ν_s (CH_3)	2854	2848	2851	2841	2820	2854	2853	2851
ν (C–H)	2726, 2675	2716, 2648	2718, 2658	2712, 2635	2749, 2714, 2637	2726, 2672	2726, 2676	2725, 2675
R(bz)	1622	1620	1626	1623	1655, 1603	1622	1625	1621
R(pz)	1558	1585	1591, 1558	1595, 1585	1587	1598	1592	1595
R(im)	1464	1471	1468	1470, 1454	1485, 1477, 1469	1483	1478	1484
δ(C–H) in-plane scissoring	1377, 1304, 1265	1352	1377, 1350, 1321, 1279, 1240, 1207	1373, 1339, 1321, 1277, 1236	1362, 1346, 1269	1377, 1320	1377, 1305	1377, 1304, 1265
δ (C–H) out-of-plane twisting	1143, 1100, 1073	1128	1169, 1124, 1078, 1061, 1017	1163, 1126, 1045	1169, 1128, 1064, 1042, 1013	1162	1154	1153
δ (C–H) out-of-plane rocking	966, 920, 880	918	949, 912	968	920, 868	969		969
δ (C–H) in-plane rocking	722, 611	735, 610	725	727	739, 685, 644, 607	722	722	722

Table 5. Parameters of diffuse reflectance spectra of complexes **V**–**VII**

Compound	λ, nm	ν, cm^{-1}	Assignment
$[CoL_2Cl_2]\cdot 0.5H_2O$ (**V**)	446	$\nu_3 = 22\,420$	$^4A_2 \rightarrow {}^4T_1(P)$
	807	$\nu_2 = 12\,390$	$^4A_2 \rightarrow {}^4T_1(F)$
$[CoL_2(NO_3)_2]\cdot 0.5H_2O$ (**VI**)	433	$\nu_3 = 23095$	$^4T_{1g}(F) \rightarrow {}^4T_{1g}(P)$
	660	$\nu_2 = 15\,150$	$^4T_{1g}(F) \rightarrow {}^4A_{2g}$
	935	$\nu_1 = 10695$	$^4T_{1g}(F) \rightarrow {}^4T_{2g}$
$[NiL_2(NO_3)_2]\cdot 0.5H_2O$ (**VII**)	395	$\nu_4 = 25316$	$^3A_{2g} \rightarrow {}^3T_{1g}(P)$
	510	$\nu_3 = 19610$	$^3A_{2g} \rightarrow {}^3T_{1g}$
	665	$\nu_2 = 15038$	$^3A_{2g} \rightarrow {}^1E_g$
	922	$\nu_1 = 10846$	$^3A_{2g} \rightarrow {}^3T_{2g}$

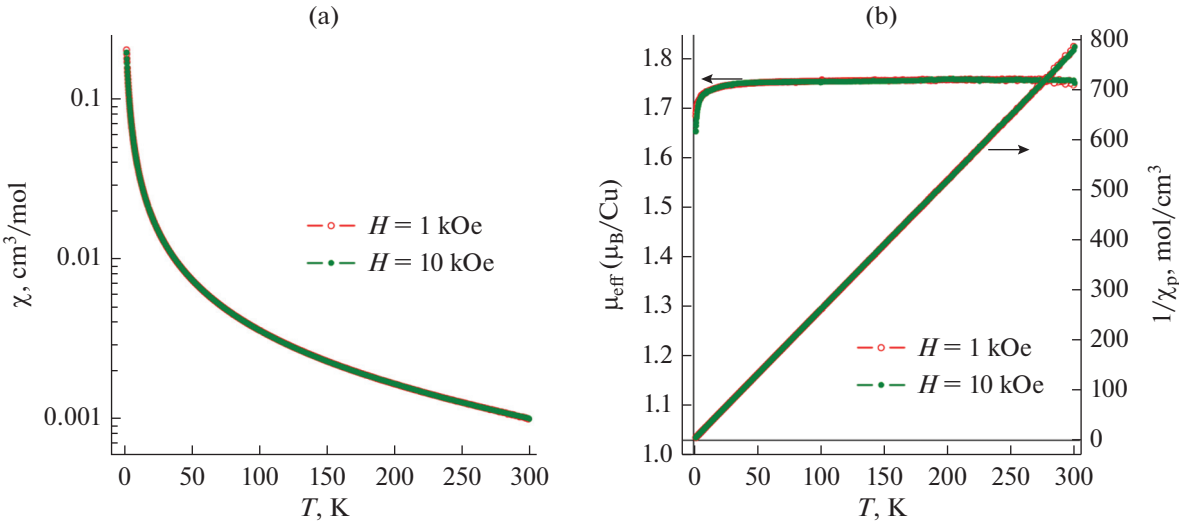

Fig. 9. (a) Temperature dependences of magnetic susceptibility of a sample of **III** measured in $H = 1$, 10 kOe magnetic fields; (b) temperature dependences of inverse susceptibility $1/\chi_p$ and effective magnetic moment μ_{eff} calculated in the approximation of non-interacting ions ($\theta = 0$).

obtained values for $M(H)$ and normalized susceptibility $\chi(H)/\chi(0)$ correspond to the behavior of Cu^{2+} ions that undergo weak antiferromagnetic interaction and can be adequately described (dashed lines) by the theoretical dependence for a system of paramagnetic centers ($S = 1/2$, $g = 2.1$) with isotropic AFM interaction $zJ/k_B = 0.30$ K. It is noteworthy that the approximation of the high-temperature data by the Curie–Weiss law gave $zJ/k_B = 0.80$ K, and the use of this value in the isotropic AFM exchange model would have given significantly underestimated magnetization (dotted line in Fig. 10). Thus, the measured field dependence of the magnetization also points to a significant (more than 2.5-fold) decrease in the effective J value at low temperature, which confirms the predominantly one-dimensional character of the exchange interaction in the crystal of **III**. The anisotropy of the exchange interaction in **III** may be attributed to the partial stacking of the planar parts of the organic ligands of neighboring molecules, but the measured J value is too low to rule out other options and to provide reliable conclusions about the mechanism of the AFM interaction.

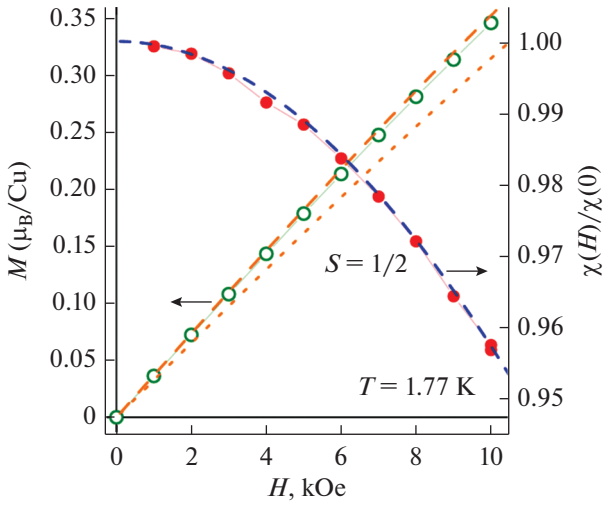

Fig. 10. Field dependences of magnetization M and normalized susceptibility $\chi(H)/\chi(0)$ for a sample of **III**. The dashed lines show approximation of the data by the theoretical dependence for a system of paramagnetic centers ($S = 1/2$, $g = 2.1$) with isotropic AFM interaction: $zJ/k_B = 0.30$ K. For comparison, the dotted line shows the theoretical magnetization of the system of the same paramagnetic centers with $zJ/k_B = 0.8$ K ($\theta \approx -0.4$ K).

Study of the effect of the compounds on the viability of HepG2 hepatocellular carcinoma cells after 48 h of exposure revealed no cytotoxic activity for either the ligand or the complexes $[CuL_2Cl_2]$ (crystals) and [CuLCl] (powder); however, incubation with the ligand and the copper(I) and copper(II) chloride complexes in the highest concentration used (50 μmol/L) caused a ≅30% decrease in the number of cells compared to the control, indicating the presence of a cytostatic effect (Fig. 11). In the case of [CuLBr], the cytostatic effect was observed for the lowest concentration used (0.2 μmol/L), with the number of cells decreasing by ≅10% relative to the control.

Under similar experimental conditions, the known carboplatin and cisplatin drugs have a more pronounced effect on HepG2 cells than the new complexes. The LC_{50} value (the concentration of a compound that causes a 50% decrease in the number of live cells compared to the control) and the IC_{50} value (the concentration of a compound that causes a 50%

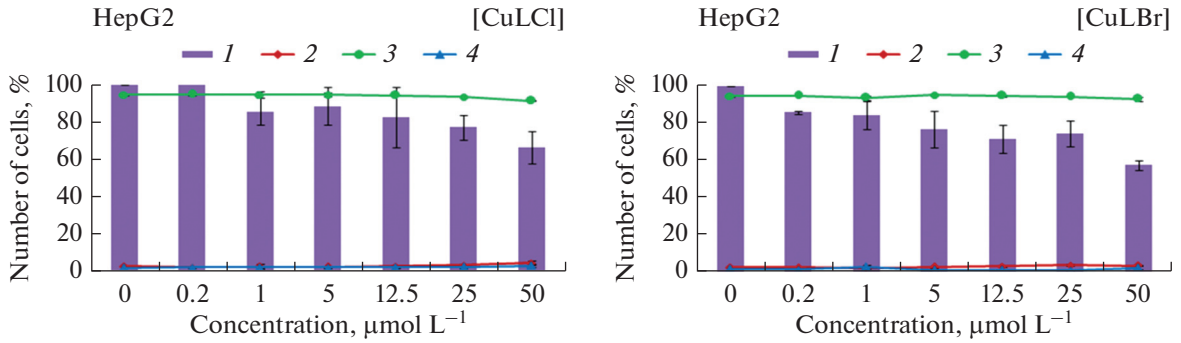

Fig. 11. Effect of the test compounds on the viability of HepG2 cells: (*1*) number of cells, (*2*) dead cells, (*3*) live cells, (*4*) apoptotic cells.

decrease in the total number of cells compared to the control) are 32 ± 2 μmol/L and 3.6 ± 0.2 μmol/L, respectively, for carboplatin and 33 ± 5 and 3.6 ± 0.2 μmol/L, respectively, for cisplatin [28]. Since HepG2 is a tumor cell line, the expression and activity of some enzymes such as CYP2C9, CYP2C19, and CYP3A4 involved in the xenobiotic metabolism are significantly lower in these cells than the expression and activity of these enzymes from normal human liver samples [33–36] However, HepG2 cells are often used for in vitro evaluation of the potential hepatotoxicity of new molecules in the initial screening stages [37]. In some cases, the carboplatin [38] and cisplatin [39] drugs possess hepatotoxicity; Therefore, the results of this study may attest to the absence of potential hepatotoxicity for the new complexes.

Thus, new copper(I), copper(II), cobalt(II), and nickel(II) complexes with 2,4-dimethylpyrazolo[1,5-a]benzimidazole were synthesized and characterized. Using HepG2 cells, it was shown that in the concentration range from 0.2 to 50 μmol/L, the ligand and the copper(I) and copper(II) chloride and bromide complexes do not show cytotoxic activity, but have a cytostatic effect on cells. The most pronounced cytotoxic effect is inherent in [CuLBr].

ACKNOWLEDGEMENTS

The authors are grateful to A.A. Shapovalova for recording the IR spectra and to I.V. Yushina for recording the diffusion reflectance spectra. The study of cytotoxic and cytostatic properties of the compounds was performed using the equipment of the Collective Use Center "Proteomic Analysis" based on the Federal Research Center for Fundamental and Translational Medicine.

FUNDING

This study was supported by the Ministry of Science and Higher Education of the Russian Federation (projects nos. 121031700313-8 and 121031700314-5). The study of the biological activity was carried out under the State Assignment of the Federal Research Center for Fundamental and Translational Medicine according to a research subject, state registration number 122032200236-1.

CONFLICT OF INTEREST

The authors of this work declare that they have no conflicts of interest.

REFERENCES

1. Selivanova, G.A. and Tretyakov, E.V., *Russ. Chem. Bull.*, 2020, vol. 69, no. 5, p. 838. https://doi.org/10.1007/s11172-020-2842-3
2. Proshin, A.N., Trofimova, T.P., Zefirova, O.N., et al., *Russ. Chem. Bull.*, 2021, vol. 70, no. 3, p. 51. https://doi.org/10.1007/s11172-021-3116-4
3. Kokorekin, V.A., Khodonov, V.M., Neverov, S.V., et al., *Russ. Chem. Bull.*, 2021, vol. 70, no. 3, p. 600. https://doi.org/10.1007/s11172-021-3131-5
4. Sadaf, H., Fettouhi, M., Fazal, A., et al., *Polyhedron*, 2019, vol. 70, p. 537. https://doi.org/10.1016/j.poly.2019.06.025
5. Munoz-Patino, N., Sanchez-Eguia, B.N., Araiza-Olivera, D., et al., *J. Inorg. Biochem.*, 2020, vol. 211, p. 111198. https://doi.org/10.1016/j.jinorgbio.2020.111198
6. Chkirate, K., Karrouchi, K., Dede, N., et al., *New J. Chem.*, 2020, vol. 44, p. 2210. https://doi.org/10.1039/C9NJ05913J
7. Masaryk, L., Tesarova, B., Choquesillo-Lazarte, D., et al., *J. Inorg. Biochem.*, 2021, vol. 217, p. 111395. https://doi.org/10.1016/j.jinorgbio.2021.111395
8. Aragón-Muriel, A., Liscano, Y., Upegui, Y., et al., *Antibiotics*, 2021, vol. 1, no. 6, p. 728. https://doi.org/10.3390/antibiotics10060728
9. Alterhoni, E., Tavman, A., Hacioglu, M., et al., *J. Mol. Struct.*, 2021, vol. 1229, p. 129498. https://doi.org/10.1016/j.molstruc.2020.129498
10. Raducka, A., Świątkowski, M., Korona-Głowniak, I., et al., *Int. J. Mol. Sci.*, 2022, vol. 23, no. 12, p. 6595. https://doi.org/10.3390/ijms23126595
11. Üstün, E., Şahin, N., Özdemir, İ., et al., *Arch. Pharm.*, 2023. https://doi.org/10.1002/ardp.202300302

12. Elkanzi, N.A., Ali, A.M., Albqmi, M., et al., *J. Organomet. Chem.*, 2022, vol. 36, no. 11, p. e6868. https://doi.org/10.1002/aoc.6868

13. Šindelář, Z. and Kopel, P., *Inorganics*, 2023, vol. 11, no. 3, p. 113. https://doi.org/10.3390/inorganics11030113

14. Rogala, P., Jabłońska-Wawrzycka, A., Czerwonka, G., et al., *Molecules*, 2022, vol. 28, no. 1, p. 40. https://doi.org/10.3390/molecules28010040

15. Helaly, A., Sahyon, H., Kiwan, H. et al., *Biointerface Res. Appl. Chem.*, 2023, vol. 13, no. 4, p. 365. https://doi.org/10.33263/BRIAC134.365

16. Sączewski, F., Dziemidowicz-Borys, E.J., Bednarski, P.J., et al., *J. Inorg. Biochem.*, 2006, vol. 100, no. 8, p. 1389. https://doi.org/10.1016/j.jinorgbio.2006.04.002

17. Volykhina, V.E. and Shafranovskaya, E.V., *Vestn. Vitebsk. Gos. Med. Un-ta*, 2009, vol. 8, no. 4, p. 6.

18. Farmer, K.J. and Sohal, R.S., *Free Radic. Biol. Med.*, 1989, vol. 7, no. 1, p. 23. https://doi.org/10.1016/0891-5849(89)90096-8

19. Rusting, R.L., *Sci. Am.,* 1992, vol 267, no. 6, p. 130. https://www.jstor.org/stable/24939339.

20. Lavrenova, L.G., Kuz'menko, T.A., Ivanova, A.D., et al., *New J. Chem.*, 2017, no. 11, p. 4341. https://doi.org/10.1039/c7nj00533d

21. Dyukova, I.I., Lavrenova, L.G., Kuz'menko, T.A., et al., *Inorg. Chim. Acta*, 2019, vol. 486, p. 406. https://doi.org/10.1016/j.ica.2018.10.064

22. Dyukova, I.I., Kuz'menko, T.A., Komarov, V.Yu., et al., *Russ. J. Coord. Chem.*, 2018, vol. 44, no. 12, p. 755. https://doi.org/10.1134/s107032841812014x

23. Ivanova, A.D., Kuz'menko, T.A., Smolentsev, A.I., et al., *Russ. J. Coord. Chem.*, 2021, vol. 47, no. 11, p. 751. https://doi.org/10.1134/S1070328421110026

24. Ivanova, A.D., Kuz'menko, T.A., Komarov, V.Yu., Glinskaya, L.A., Sheludyakova, L.A., Klyushova, L.S., and Lavrenova, L.G., *Russ. Chem. Bull.*, 2021, vol. 70, no. 8, p. 1550. https://doi.org/10.1007/s11172-021-3251-y

25. Kuz'menko, V.V., Komissarov, V.N., and Simonov, A.M., *Chem. Heterocycl. Comp.*, 1980, vol. 16, no. 6, p. 34.

https://doi.org/10.1007/pl00020455

26. APEX2 (version 2012.2-0), SAINT (version 8.18c), and SADABS (version 2008/1), in *Bruker Advanced X-ray Solutions*, Madison: Bruker AXS Inc., 2000–2012.

27. Sheldrick, G.M., *Acta Crystallogr., Sect. C: Struct. Chem.*, 2015, vol. 71, p. 3. https://doi.org/10.1107/S2053229614024218

28. Klyushova, L.S., Golubeva, Yu.A., Vavilin, V.A., and Grishanova, A.Yu., *Acta Biomed. Sci.*, 2022, vol. 7, no. 5-2, p. 31. https://doi.org/10.29413/ABS.2022-7.5-2.4

29. Nakamoto, K., *Infrared and Raman Spectra of Inorganic and Coordination Compounds*, New York: Wiley, 1986.

30. Lever, A.B.P., *Inorganic Electronic Spectroscopy*, Amsterdam: Elsevier, 1985.

31. Lavrenova, L.G., Ivanova, A.I., Glinskaya, L.A., et al., *Chem. Asian J.*, 2023, vol. 18, p. e202201200. https://doi.org/10.1002/asia.202201200

32. Bonner, J.C. and Fisher, M.E., *Phys. Rev.*, 1964, vol. 135, no. 3A, p. A640. https://doi.org/10.1103/PhysRev.135.A640

33. Wilkening, S., Stahl, F., and Bader, A., *Drug. Metab. Dispos.*, 2003, vol. 31, no. 8, p. 1035. https://doi.org/10.1124/dmd.31.8.1035

34. Donato, M.T., Tolosa, L., and Gómez-Lechón, M.J., *Methods Mol. Biol.*, 2015, no. 1250, p. 77. https://doi.org/10.1007/978-1-4939-2074-7_5

35. Nekvindova, J., Mrkvicova, A., Zubanova, V., et al., *Biochem. Pharmacol.*, 2020, vol. 177, no. 113912. https://doi.org/10.1016/j.bcp.2020.113912

36. Shen, H., Wu, H., Sun, F., et al., *Bioengineered*, 2021, vol. 12, no. 1, p. 240. https://doi.org/10.1080/21655979.2020.1866303

37. Donato, M.T., Jover, R., and Gómez-Lechón, M.J., *Curr. Drug. Metab.*, 2013, vol. 14, no. 9, p. 946. https://doi.org/10.2174/1389200211314090002

38. *LiverTox: Clinical and Research Information on Drug-Induced Liver Injury [Internet]. Carboplatin*, Bethesda: National Institute of Diabetes and Digestive and Kidney Diseases, 2012. https://www.ncbi.nlm.nih.gov/books/NBK548565/.

39. *LiverTox: Clinical and Research Information on Drug-Induced Liver Injury [Internet]. Cisplatin*, Bethesda: National Institute of Diabetes and Digestive and Kidney Diseases, 2012. https://www.ncbi.nlm.nih.gov/books/NBK548160/.

Translated by Z. Svitanko